J|A|C|S
ARTICLES
Published on Web 09/29/2006

Homogeneous Decomposition of Aryl- and Alkylimido Precursors for the Chemical Vapor Deposition of Tungsten Nitride: A Combined Density Functional Theory and Experimental Study

Yong Sun Won,[†] Young Seok Kim,[†] Timothy J. Anderson,[†,*] Laurel L. Reitfort,[‡] Ion Ghiviriga,[‡] and Lisa McElwee-White[‡,*]

Contribution from the Department of Chemical Engineering, University of Florida, Gainesville, Florida 32611-6005, and Department of Chemistry, University of Florida, Gainesville, Florida 32611-7200

Received March 30, 2006; Revised Manuscript Received July 18, 2006; E-mail: lmwhite@chem.ufl.edu

Abstract: MOCVD growth of tungsten nitride (WN_x) and tungsten carbonitride (WN_xC_y) thin films has been reported from the complexes $Cl_4(CH_3CN)W(NR)$ (**1**: R = Ph; **2**: R = ^{i}Pr; **3**: R = C_3H_5). To evaluate the role of the imido substituent in film growth, gas-phase homogeneous decomposition of precursor molecules was investigated using density functional theory (DFT) calculations. Computational results and NMR kinetics of acetonitrile exchange by **2** in solution verified that dissociation of the acetonitrile ligand should be facile for **1**−**3** in the temperature range used for film growth (>450 °C). A computational search for transition states for cleavage of W−Cl bonds in the presence of H_2 carrier gas was consistent with a σ-bond metathesis pathway. Natural bonding orbital (NBO) analysis and bond energy calculations indicated that **1** has a stronger N−C(imido) bond and a slightly weaker W−N bond than **2** and **3**, suggesting a greater role for W−N bond cleavage in depositions from **1**. These results are consistent with mass spectrometric fragmentation patterns from **1**−**3** and low nitrogen content in films deposited from **1** as compared to those from **2** and **3**.

Introduction

Although Al-based metalization schemes have historically been used in integrated circuits (ICs), the more recent use of copper is motivated by its higher electrical conductivity and increased resistance to electromigration. The high diffusivity of copper in silicon ($D_{Cu} \sim 2 \times 10^{-5}$ cm^2/s at 500 °C)[1,2] coupled with its low solubility, however, leads to extensive redistribution of Cu and its accumulation at extended defects, which degrades device performance and process yields. To overcome the problem of copper contamination, thin films acting as diffusion barriers are used.[3,4] Besides having good resistance to diffusion, barrier films should be structurally and thermally stable, exhibit good adhesion to both copper and dielectric layers, be nonreactive with copper, have low resistivity, and be resistant to thermal and mechanical stresses. Tungsten nitride (WN_x)[5−11] and tungsten carbonitride (WN_xC_y)[12−14] are promising candidates for barrier materials based on these criteria. Recently, we reported metal−organic chemical vapor deposition (MOCVD) growth of WN_x and WN_xC_y thin films using a series of related single source precursors: the phenylimido complex $Cl_4(CH_3CN)W(NPh)$ (**1**),[15] the isopropylimido complex $Cl_4(CH_3CN)W(N^iPr)$ (**2**),[16] and the allylimido complex $Cl_4(CH_3CN)W(NC_3H_5)$ (**3**).[17] Analyses of mass spectra of **1**−**3** obtained via positive ion electron-impact (EI) and negative ion electron-capture chemical ionization (NCI) provided insight into probable precursor decomposition pathways while the activation energies for film growth were correlated to estimated N−C bond dissociation energies within the imido ligand. Properties of the deposited films were discussed in the context of probable

[†] Department of Chemical Engineering.
[‡] Department of Chemistry.

(1) Istratov, A. A. *J. Electrochem. Soc.* **2000**, *149* (1), G21−G30.
(2) Broniatowski, A. *Phys. Rev. Lett.* **1989**, *62*, 3074−3077.
(3) Nicolet, M. A. *Thin Solid Films* **1978**, *52*, 415−443.
(4) Istratov, A. A.; Weber, E. R. *Electrochem. Soc. Conf. Proc.* **2000**, *2000-27*, 90−111.
(5) Nakajima, K.; Akasaka, Y.; Miyano, K.; Takahashi, M.; Suehiro, S.; Suguro, K. *Appl. Surf. Sci.* **1997**, *117/118*, 312−316.
(6) Nakajima, T.; Watanabe, K.; Watanabe, N. *J. Electrochem. Soc.* **1987**, *134*, 3175−3178.
(7) Ivanova, A. R.; Galewski, C. J.; Sans, C. A.; Seidel, T. E.; Grunow, S.; Kumar, K.; Kaloyeros, A. E. *Mater. Res. Soc. Symp. Proc.* **1999**, *564*, 321−326.
(8) Galewski, C.; Seidel, T. *Eur. Semicond.* **1999**, 31−32.
(9) Shaw, M. J.; Grunow, S.; Duquette, D. J. *J. Electron. Mater.* **2001**, *30*, 1602−1608.
(10) Uekubo, M.; Oku, T.; Nii, K.; Murakami, M.; Takahiro, K.; Yamaguchi, S.; Nakano, T.; Ohta, T. *Thin Solid Films* **1996**, *286*, 170−175.
(11) Kaloyeros, A. E.; Eisenbraun, E. *Annu. Rev. Mater. Sci.* **2000**, *30*, 363−385.
(12) Kim, S.-H.; Oh, S. S.; Kim, K.-B.; Kang, D.-H.; Li, W.-M.; Haukka, S.; Tuominen, M. *Appl. Phys. Lett.* **2003**, *82*, 4486-4488.
(13) Kim, S.-H.; Oh, S. S.; Kim, H.-M.; Kang, D.-H.; Kim, K.-B.; Li, W.-M.; Haukka, S.; Tuominen, M. *J. Electrochem. Soc.* **2004**, *151*, C272−C282.
(14) Li, W.-M.; Tuominen, M.; Haukka, S.; Sprey, H.; Raaijmakers, I. J. *Solid State Technol.* **2003**, *46*, 103−104, 106.
(15) Bchir, O. J.; Green, K. M.; Hlad, M. S.; Anderson, T. J.; Brooks, B. C.; Wilder, C. B.; Powell, D. H.; McElwee-White, L. *J. Organomet. Chem.* **2003**, *684*, 338−350.
(16) Bchir, O. J.; Johnston, S. W.; Cuadra, A. C.; Anderson, T. J.; Ortiz, C. G.; Brooks, B. C.; Powell, D. H.; McElwee-White, L. *J. Cryst. Growth* **2003**, *249*, 262−274.
(17) Bchir, O. J.; Green, K. M.; Ajmera, H. M.; Zapp, E. A.; Anderson, T. J.; Brooks, B. C.; Reitfort, L. L.; Powell, D. H.; Abboud, K. A.; McElwee-White, L. *J. Am. Chem. Soc.* **2005**, *127*, 7825−7833.

decomposition pathways postulated from the mass spectra. On the basis that no ions containing the acetonitrile ligand were detected by mass spectrometry in either mode, we proposed that facile dissociation of the acetonitrile ligand (CH_3CN) was the first step in the deposition. The pathway for loss of chloride from the precursor was still unclear, although some information could be obtained from observation of HCl (but not Cl_2 or alkyl/aryl chlorides) in the reactor effluent by RGA (residual gas analyzer). Loss of chloride must be efficient, as Cl was not present in the films to the limit of detection by AES (Auger electron spectroscopy).

The only other information on reaction pathways for this set of single source precursors is that indirectly inferred from the measured temperature dependence of the growth rate.[15−17] The deposition of compounds **1** and **2** showed two growth rate regimes. At low temperature (<550 and 600 °C, respectively) Arrhenius behavior was observed with estimated activation energy of 1.41 and 0.84 eV, respectively. At higher temperature the growth rate increased only slightly with temperature, characteristic of mass transfer limited growth. Compound **3** showed only one regime in the temperature range 450 to 650 °C with weak temperature dependence and activation energy of only 0.15 eV, which is outside the normal range associated with surface reaction controlled CVD. The different values of the estimated activation energy in the low temperature regime suggest that the imido ligand is involved in the rate limiting step, which most probably is a surface reaction for compounds **1** and **2**. The regime of weak growth rate temperature dependence is indicative of mass transfer limited growth. The temperature at which this transition occurs, of course, is dependent on the reactor design and operating conditions. At even higher temperature (>800, 750, and 650 °C for compounds **1**, **2**, and **3**) the growth rate decreased, and for compounds **2** and **3**, black particle deposition was observed. Decreased growth rate and particle deposition suggest parasitic gas-phase reactions are important, possibly leading to homogeneous nucleation of particles. It is noted that the film composition and measured resistivity showed an even more complex behavior with deposition temperature. The reaction pathways for these single source precursors are very likely complex and involve both gas-phase and surface reactions with their relative rates dependent on the operating conditions. Although surface reactions are expected to be important, particularly at low deposition temperature, this paper focuses on the gas-phase reaction chemistry, which is also expected to be important to deposition.

Computational chemistry is an alternative tool for investigation of the decomposition mechanism of metal−organic CVD precursors. In this study, we present density functional theory (DFT) calculations used to analyze bonding in the alkyl- and arylimido complexes **1**−**3**. In addition, computational study of the CH_3CN cleavage step by means of statistical thermodynamics is presented. Cleavage of the W−Cl bonds by σ-bond metathesis with H_2 has also been examined computationally, and a pathway based on calculated transition state structures is proposed. The computational results are compared to experimental data from kinetics of acetonitrile exchange of **2** as determined by NMR and mass spectrometry of **1**−**3**.

Experimental Section

Computational Methods. All calculations were carried out using the GAUSSIAN 03 program, along with B3LYP DFT method and split basis sets (LanL2DZ for tungsten and 6-311G(d) for other elements).[18−20] Full geometry optimization was carried out for all species. Transition states (TS) were optimized using the Berny algorithm as implemented in the GAUSSIAN 03 program. Harmonic vibration frequencies were calculated for each structure and used as the basis for computing enthalpy and Gibbs energy for thermochemical analysis.[18] Atomic charges and Wiberg indices were evaluated using natural bond orbital (NBO) analysis. The GaussView, MolDen, and gOpenMol programs were used for the visualization of the results.[21,22]

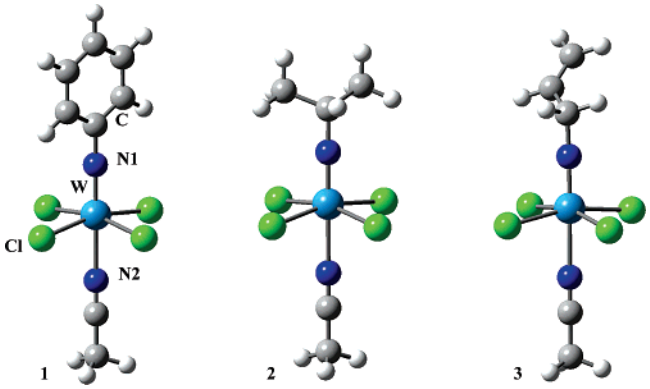

Figure 1. Optimized geometries for complexes **1**−**3**.

NMR Kinetics of Acetonitrile Exchange in 2. Compound **2** was prepared as previously described.[23] The sample for the exchange study was prepared in the drybox by dissolving complex **2** and an equivalent amount of acetonitrile in $CDCl_3$. The ^1H NMR spectrum of this sample at −20 °C displayed the signals for **2** [δ (ppm) 7.14 (hp, 1H), 2.58 (s, 3H) 1.70 (d, 6H)] together with free acetonitrile (2.11 ppm) in a ratio of 1:3. The exchange of **2** with acetonitrile in the solution was monitored by ^1H NMR in the temperature range −54 to 34 °C. The exchange rate k (see Supporting Information) was determined by line shape analysis in the temperature range −6 to 34 °C. A plot of $\ln(k/T)$ vs $1/T$ afforded the activation enthalpy (18.52 ± 0.14 kcal/mol) and entropy (15.8 ± 0.5 cal/mol·K) for the exchange of acetonitrile by **2**.

The NMR spectra were recorded on a Varian Inova at 500 MHz for proton, equipped with a 5 mm indirect detection probe, with z-axis gradients. The variable temperature spectra were recorded on automation. To achieve temperature stability, for each temperature step of 2 °C, a preacquisition delay of 1500 s was followed by shimming on the lock level. The spectra were collected in 16 transients, with an acquisition time of 5 s. No relaxation delay and no apodization were used. The actual temperature was measured by running a standard of methanol under the same conditions. The simulation of the spectra with exchange was done using gNMR.[24]

Results and Discussion

Optimized Geometries. The optimized geometries for complexes **1**−**3**, are, as expected, very similar (Figure 1, Table 1). All three complexes exhibit octahedral coordination at the tungsten center. Their N−W−Cl bond angles are greater than the ideal 90°, as expected for an octahedral complex with a single multiply bonded ligand.[25] The W−N bond lengths and the bond angles about the tungsten center are in reasonable

(18) Frisch, M. J.; et al. *Gaussian 03, Revision B.04*, 2004.
(19) Becke, A. D. *J. Chem. Phys.* **1993**, *98*, 1372.
(20) Lee, W. Y.; Strife, J. R.; Veltri, R. D. *J. Am. Ceram. Soc.* **1992**, *75*, 2803.
(21) Laaksonen, L. *J. Mol. Graph.* **1992**, *10*, 33−34.
(22) Bergman, D. L.; Laaksonen, L.; Laaksonen, A. *J. Mol. Graph. Model.* **1997**, *15*, 301−306.
(23) Johnston, S. W.; Ortiz, C. G.; Bchir, O. J.; Zhang, Y.; McElwee-White, L.; Anderson, T. J. In *Chemical Vapor Deposition: CVD XV (15th)*; Allendorf, M. D., Besmann, T. M., Eds.; Electrochemical Society: Pennington, NJ, 2000; Vol. 2000-13, pp 268−276.
(24) *gNMR*; Adept Scientific PLC:·Amor Way, Letchworth, Herts, SG6 IZA, UK., 2000

Table 1. Calculated Bond Lengths (Å) and Bond Angles (deg) for Complexes **1**−**3**

	1	2	3	
	calcd	calcd	calcd	exp[b]
W−Cl[a]	2.380	2.377	2.375	2.333
W−N1	1.738	1.715	1.716	1.687 (9)
W−N2	2.262	2.347	2.342	2.308 (8)
C−N1	1.363	1.428	1.425	1.508 (17)
Cl−W−N1[a]	95.9	98.1	98.1	97.4
W−N1−C	180.0	179.6	177.7	167 (2)

[a] Average value for the four equivalent chlorides. [b] Experimental values from the X-ray crystal structure of **3**.[17]

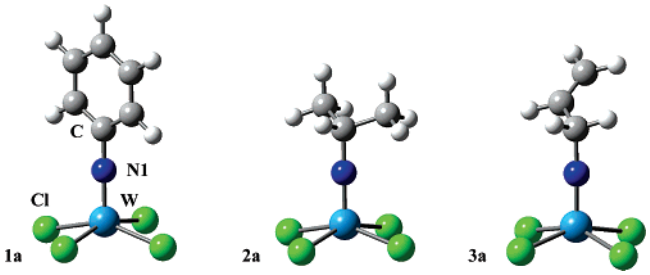

Figure 2. Optimized geometries of complexes **1a**−**3a**.

accord with experimental values obtained for related complexes by X-ray diffraction[17,26,27] and standard literature values.[28] Minor differences in bond lengths and angles can be attributed, at least in part, to crystal packing forces that are not present in gas-phase calculations.

The geometry optimizations of complexes **1**−**3** revealed additional local minima associated with rotation of the imido substitutent. As an example, two local mimina were found for the phenylimido complex: in one, the phenyl ring is coplanar with a trans pair of chlorines, while in the other, the plane of the phenyl ring bisects the Cl−W−Cl angle. The energy difference between these two conformations was only 0.077 kcal/mol. The lack of an electronic barrier for rotation of a planar ligand is characteristic of octahedral *trans*-$ML_4L'L''$ complexes, in which the 4-fold local symmetry renders the d_{xz} and d_{yz} orbitals degenerate in the ML_4L' fragment.

In preparation for assessment of the chemistry of **1**−**3** following loss of the labile acetonitrile ligand, their coordinatively unsaturated derivatives $Cl_4W(NPh)$ (**1a**), $Cl_4W(N^iPr)$ (**2a**), and $Cl_4W(NC_3H_5)$ (**3a**) were also subjected to computational geometry optimization (Figure 2, Table 2). Due to the lowered electron density around the metal upon loss of the CH_3CN ligand, the W−Cl and W−N bond lengths in **1a**−**3a** are shorter than in the coordinatively saturated **1**−**3**. Increased N−W−Cl bond angles are a result of distortion toward a square pyramidal geometry with the strong trans influence imido ligand in the apical position.

Note that in all six complexes (**1**−**3** and **1a**−**3a**), the N(imido)−C bond lengths follow the trend expected on the basis of the hybridization at carbon. For the phenyl compounds **1** and **1a**, the ipso carbon is sp^2 hybridized, leading to a prediction

Table 2. Calculated Bond Lengths (Å) and Bond Angles (deg) for Complexes **1a**−**3a**

	1a	2a	3a
W−Cl[a]	2.344	2.346	2.345
W-N1	1.716	1.702	1.703
C−N1	1.372	1.440	1.436
Cl−W−N1[a]	102.5	102.6	102.7
W−N1−C	180.0	179.0	178.3

[a] Average value for the four equivalent chlorides.

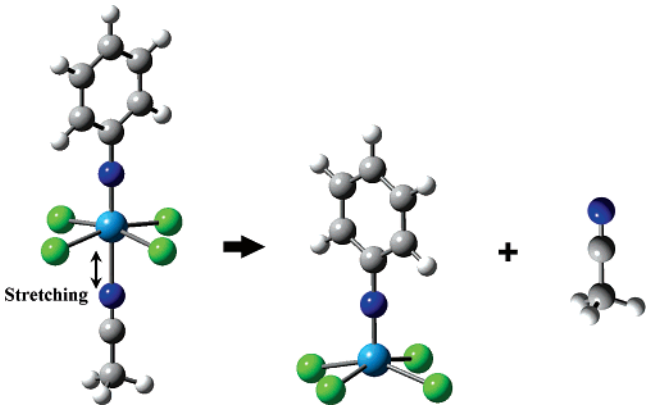

Figure 3. Assumed vibrational mode leading to CH_3CN dissociation from **1**.

that the N(imido)−C(sp^2) bond length will be shorter than the N(imido)-C(sp^3) bond lengths in the isopropyl- and allylimido complexes **2**−**3** and **2a**−**3a**. Experimental N(imido)−C bond lengths obtained by X-ray crystallographic structure determination follow the same trend. A search of the Cambridge Structural Database[29] yielded a mean N(imido)−C(sp^2) bond length of 1.40 Å for 29 tungsten phenylimido complexes. A similar analysis for alkylimido complexes afforded a mean N(imido)−C (sp^3) bond length of 1.46 Å for 14 tungsten *tert*-butylimido complexes, while the less sterically hindered ethylimido complexes averaged an N−C bond length of 1.43 Å (6 structures).

Dissociation of Acetonitrile from 1, 2, and 3. We previously postulated initial dissociation of the CH_3CN ligand from **1**−**3** during film growth on the basis of the strong trans influence of imido ligands,[25,30] which has been correlated to trans effects in the dissociative reactions of imido complexes.[31] This decomposition mechanism for **1**−**3** had been previously discussed in the context of their mass spectra, in which the highest *m*/*z* values in both positive and negative modes correspond to ions from which CH_3CN has been lost.[15−17] Calculations of the frequencies for the W−N(nitrile) stretching mode shown in Figure 3 yielded values of 190 cm^{-1} for **1**, 194 cm^{-1} for **2**, and 191 cm^{-1} for **3**. The frequency of 190 cm^{-1} is equivalent to the vibrational temperature (Θ_v) of 274 K, supporting the hypothesis that acetonitrile dissociation from **1**−**3** would be kinetically facile at the typical film deposition temperature in the range 450 to 750 °C.

Assuming that CH_3CN dissociation occurs via a simple stretching mode, statistical thermodynamics was used to estimate values of $\Delta H_f°$ and $\Delta S_f°$ of complexes **1**−**3**, **1a**−**3a**, and CH_3-

(25) Nugent, W. A.; Mayer, J. M. *Metal−Ligand Multiple Bonds*; Wiley: New York, 1988.
(26) Görge, A.; Dehnicke, K.; Fenske, D. *Z. Naturforsch. (B)* **1988**, *43*, 677−681.
(27) Bradley, D. C.; Errington, R. J.; Hursthouse, M. B.; Short, R. L.; Ashcroft, B. R.; Clark, G. R.; Nielson, A. J.; Rickard, C. E. F. *J. Chem. Soc.,Dalton Trans.* **1987**, 2067−2075.
(28) Orpen, A. G.; Brammer, L.; Allen, F. H.; Kennard, O.; Watson, D. G.; Taylor, R. *J. Chem. Soc., Dalton Trans.* **1989**, S1−S83.
(29) Allen, F. H. *Acta Crystallogr.* **2002**, *B58*, 380−388.
(30) Vaughan, W. M.; Abboud, K. A.; Boncella, J. M. *Organometallics* **1995**, *14*, 1567−1577.
(31) Hogarth, G.; Richards, I. *Dalton Trans.* **2005**, 760−773.

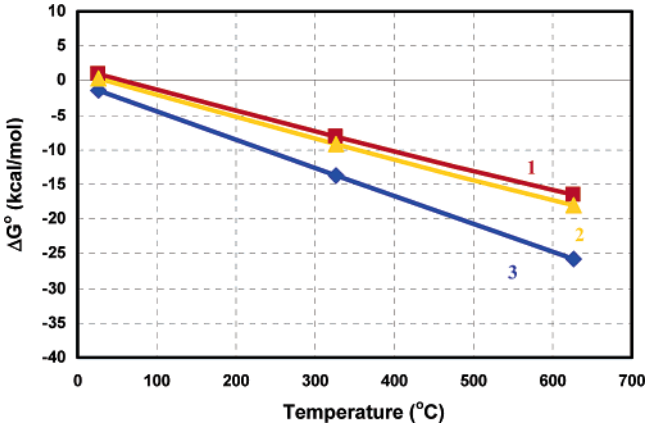

Figure 4. Calculated standard Gibbs energy change ($\Delta G°$) vs temperature for CH_3CN dissociation from complexes **1**−**3**.

Table 3. Calculated Reaction Enthalpies for CH_3CN Dissociation from Complexes **1**−**3**

compound	BDE (kcal/mol)[a]
1	10.4
2	10.2
3	11.0

[a] For compound **X**, calculated as $\Delta H_f°$(**Xa**) + $\Delta H_f°$(CH_3CN) − $\Delta H_f°$(**X**).

CN, allowing $\Delta H°$ and $\Delta G°$ for the cleavage reaction to be calculated. A plot of $\Delta G°$ vs temperature and $\Delta H°$ for dissociation of acetonitrile from **1**−**3** are shown in Figure 4 and Table 3, respectively. Here, $\Delta\Delta H°$ (**1a**) + $\Delta\Delta H°$ (CH_3CN) − $\Delta\Delta H°$ (**1**) can be regarded as approximately equal to the activation energy for CH_3CN ligand cleavage from **1** because the transition state for this endothermic reaction should be product-like in character. Note that at temperatures within the film growth range, $\Delta G°$ is negative, indicating that acetonitrile loss is thermodynamically favorable. These calculations are consistent with experimental data that implies dissociation of CH_3CN as the first step in film growth from **1**−**3** at temperature above 450 °C.

To obtain experimental values for the activation energy of CH_3CN dissociation from complex **2**, ^1H NMR kinetics were used to study the exchange of the acetonitrile ligand with free CH_3CN in $CDCl_3$ solution. Upon lowering the temperature to −20 °C, both bound and free acetonitrile could be detected in the ^1H NMR spectra. As the temperature was raised, the bound and free acetonitrile signals coalesced. The exchange rate k was determined by line shape analysis in the temperature range −6 to 34 °C. A plot of $\ln(k/T)$ vs $1/T$ (see Supporting Information) yielded an activation energy of 18.52 ± 0.14 kcal/mol and an entropy of activation of 15.8 ± 0.5 cal/mol·K for the exchange of acetonitrile. Since the first-order kinetics of the process are consistent with a dissociative mechanism for the exchange process, those values correspond to $\Delta H^‡$ and $\Delta S^‡$ for loss of CH_3CN from isopropylimido complex **2**. Given that the experimental values were obtained in solution while the calculated values are for a gas-phase process, the agreement between them is reasonable.

Cleavage of W−Cl Bonds in 1−3. According to the RGA (residual gas analyzer) data obtained from the reactor effluent during deposition of films from imido complexes **1** and **2** in the presence of H_2 carrier gas,[15,32] HCl was the only detected chlorine-containing decomposition product. Interestingly, suboptimal films can also be grown under N_2 carrier gas but RGA of the reactor effluent from growths in N_2 shows the presence of H_2 along with the HCl.[32] Apparently, H_2 generated by cracking of solvent or precursor fragments undergoes reaction even when no H_2 is added to the system. Given the high oxidation state of the tungsten centers in **1** and **2**, it is noteworthy that the reductive elimination product Cl_2 was not observed. In addition, chlorine was not present in the deposited WN_x films within the detection limits of AES (Auger electron spectroscopy), suggesting that removal of chlorine from the intermediates as HCl is an efficient process. Thus, the mechanistic

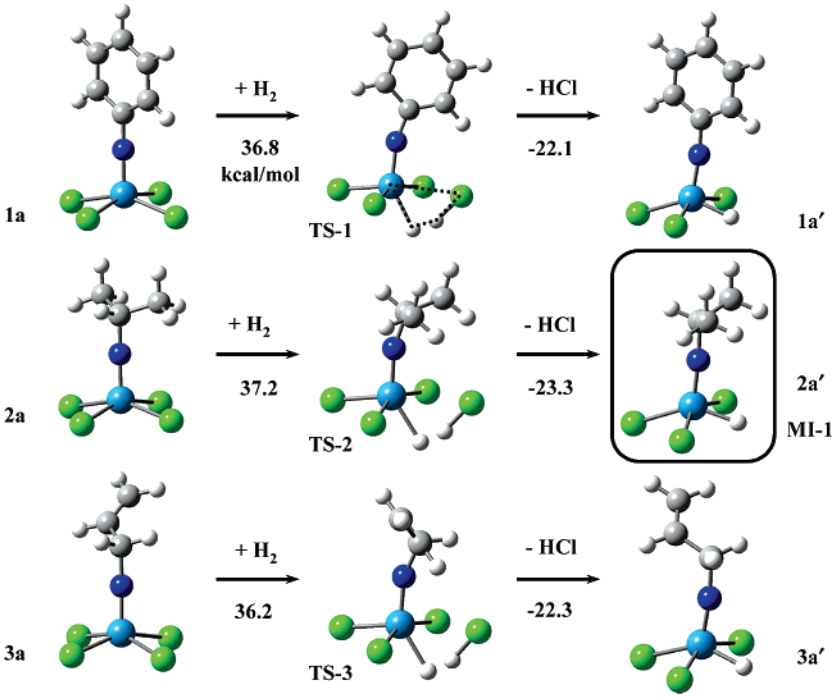

Figure 5. Calculated transition states (center) and products (right) for σ-bond metathesis of **1a**−**3a** with hydrogen. Energy values are in kcal/mol.

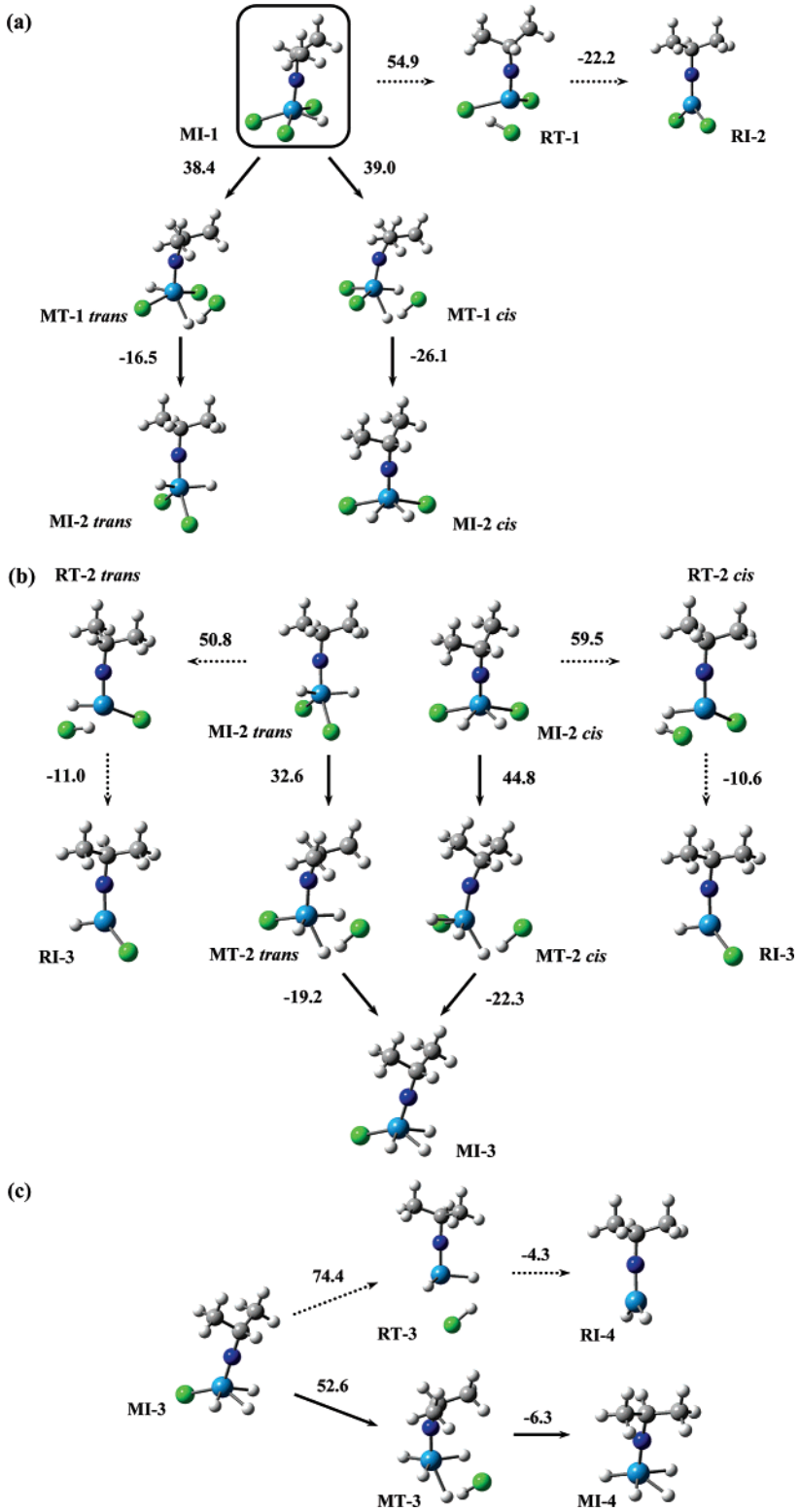

Figure 6. Calculated transition states and intermediates for possible σ-bond metathesis (solid arrows) and reductive elimination (dotted arrows) steps on reaction pathway of **2a** with H_2. In compound designations: M = metathesis; R = reductive elimination; T = transition state; I = intermediate. (a) Reaction with second chloride of **2a**. (b) Reaction with third chloride of **2a**. (c) Reaction of last chloride of **2a**. See Figure 5 for initial reaction of **2a** with H_2 to yield MI-1.

pathways from imido complexes **1**−**3** to HCl are of interest and have been investigated computationally.

Conversion of the chloride ligands to HCl under film deposition conditions suggests involvement of the H_2 carrier gas in cleavage of the W−Cl bonds. The most common pathways for reaction of H_2 with organometallic complexes include the following: (1) oxidative addition, (2) coordination of H_2 followed by transfer of an acidic proton, and (3) σ-bond metathesis. Oxidative addition is precluded by the d^0 electron count of **1**−**3** and **1a**−**3a**, and as expected, local minima associated with formation of the dihydride could not be found. Although precoordination of H_2 as a σ-complex has been

reported to lie in a shallow well in prior DFT studies of electron poor d^0 species,[33] we could not locate such a minimum for approach of H_2 to **1a**−**3a**.

For d^0 transition metal complexes, the preferred reaction pathway with H_2 is σ-bond metathesis, in which ligand exchange occurs via a four-center transition state.[33,34] Observation of σ-bond metathesis is generally confined to those systems where oxidative addition is not a viable pathway. Figure 5 shows the transition states for σ-bond metathesis of **1a**−**3a** with H_2 and local minimum geometries for the metal hydride products $Cl_3HW(NR)$ (**1a′**−**3a′**). Precedent for the existence of chloro hydrido tungsten imido complexes can be found in the coordinatively unsaturated reactive intermediate $(^tBu_3SiN)_2WHCl$, which was postulated on the basis of trapping products.[35] Each transition state depicted in Figure 5 exhibited the requisite single negative force constant with the corresponding vibrational mode leading to formation of the metal hydride and HCl. The reactions are endothermic, with activation energy of approximately 37 kcal/ mol, which will be accessible in the reported growth temperature range 450 to 750 °C. To our knowledge, σ-bond metathesis of a metal chloride with H_2 to yield a metal hydride and HCl has not been previously reported. However, under the high temperature and H_2 flux of the CVD reaction conditions, this reaction appears to be a viable pathway to the experimentally observed chloride-free films and HCl byproduct.

Given the lack of experimental precedent for σ-bond metathesis between a metal chloride and H_2, we carried out calculations with additional basis functions to test the results. The calculations summarized in Figure 5 were performed with the 6-311G(d) basis set for non-tungsten atoms. A similar calculation was carried out for the isopropylimido complex **2a** using the 6-311G(d,p) basis set. $\Delta H^{\ddagger}$ decreased to 33.1 kcal/ mol upon addition of diffuse p functions, but the computational results were essentially unchanged.

Figure 6 depicts possible σ-bond metathesis intermediates for successive substitution of chlorides by hydrides and possible pathways for reductive elimination of HCl from the hydride complexes. As substitution can lead to either the trans (MI-2A) or cis (MI-2B) isomer of $H_2Cl_2W(N^iPr)$, several reaction manifolds were considered. The activation energy for the second or third σ-bond metathesis was roughly equivalent to that for the first σ-bond metathesis (around 38 ∼ 45 kcal/mol). All of these values were significantly less than those for reductive elimination of HCl from the corresponding intermediate. Although the activation energy for the fourth chloride loss by σ-bond metathesis (ca. 53 kcal/mol) was higher than the first three, it was still competitive with the calculated activation energy for reductive elimination of HCl (ca. 74 kcal/mol).

Bond Dissociation Energies for W−N(imido) and N(imido)−C in Complexes 1−3. Growth of WN_x from **1**−**3** requires not only dissociation of the acetonitrile and chloride ligands (vide supra) but also cleavage of the N−C bond in the imido ligand. We have previously demonstrated that the apparent growth kinetics and composition of WN_x films grown from **1**−**3** can be correlated with the bond dissociation energies of the N(imido)−C bond in the precursor.[17] In an effort to understand the effects of bonding within the imido moiety on precursor decomposition under film growth conditions, a computational investigation was carried out.

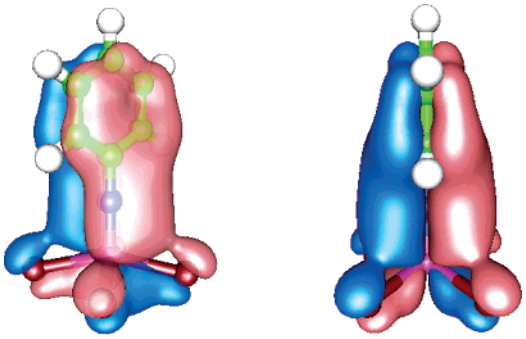

Figure 7. Conjugation of N lone pair to metal d and through the phenyl ring as observed in the HOMO-18. Contours are drawn at ± 0.015 au.

As seen in Tables 1 and 2, bonding throughout the imido moiety reflects the difference of **1**, which exhibits conjugation between the phenyl group and the imido nitrogen, from **2** and **3**, which bear saturated carbons at the C−N1 linkage. In **1**, donation of the p-type nitrogen lone pair into an empty metal d orbital is attenuated by conjugation of the N p-orbital into the phenyl ring (Figure 7). This effect weakens the W−N1 bonding of **1** with respect to that in **2** and **3**, for which such conjugation into the alkyl group is not possible. The result can be seen in the longer W−N1 bond in **1** (1.737 Å) in comparison to those of **2** and **3** (1.724 Å). A related effect can be seen in the N1−C bond lengths, where the N1−C(sp^2) length in phenylimido complex **1** (1.380 Å) is, as expected, shorter than the N1−C(sp^3) distances in alkylimido complexes **2** and **3** (1.441 and 1.444 Å).

Additional information on bonding of the imido ligands of **1**−**3** was obtained using natural bonding orbital (NBO) analysis. Figure 8 depicts the atomic charge of each atom calculated from natural population analysis (NPA) and the Wiberg bond index for bonds of interest. As expected, the calculated bond order of the N−C(phenyl) bond of **1** is higher than those of the N−C(alkyl) bonds of **2** and **3**. The Wiberg bond indices for the W−N1 bonds of **1**−**3** also support the relative bond strengths inferred from bond distances, with the longer W−N1 bond of **1** exhibiting a significantly lower bond index than those of **2** and **3**.

To make a quantitative comparison of the N1−C bond energies in **1**−**3** and **1a**−**3a**, the energetics of the reaction depicted in Figure 9 were determined by using statistical thermodynamics to obtain values for $\Delta H_f°$ and $\Delta G_f°$ of complexes **1a**−**3a** and their products of cleavage at the W−N and C−N bonds, allowing $\Delta H°$ and $\Delta G°$ for the reactions to be calculated. Acetonitrile-free complexes **1a**−**3a** were used for this calculation because the lability of the acetonitrile ligand suggests its dissociation to be the first step of the decomposition of **1**−**3** under film deposition conditions (vide supra). The homolytic cleavage of the N(imido)−C bonds required for calculating the bond dissociation energies resulted in open shell products that were treated as doublets. In the cases of W−N1 cleavage, the products were treated as triplets. The basis set superposition error was corrected, although it was less than 5% compared to the overall $\Delta H°$ value in each calculation. Table 4 summarizes the estimated bond dissociation enthalpy values.

(32) Bchir, O. J.; Green, K. M.; Hlad, M. S.; Anderson, T. J.; Brooks, B. C.; McElwee-White, L. *J. Cryst. Growth* **2004**, *261*, 280−288.
(33) Folga, E.; Ziegler, T. *Can. J. Chem.* **1992**, *70*, 333−342.
(34) Cundari, T. R.; Stevens, W. J.; Sommerer, S. O. *Chem. Phys.* **1993**, *178*, 235−243.
(35) Holmes, S. M.; Schafer, D. F.; Wolczanski, P. T.; Lobkovsky, E. B. *J. Am. Chem. Soc.* **2001**, *123*, 10571−10583.

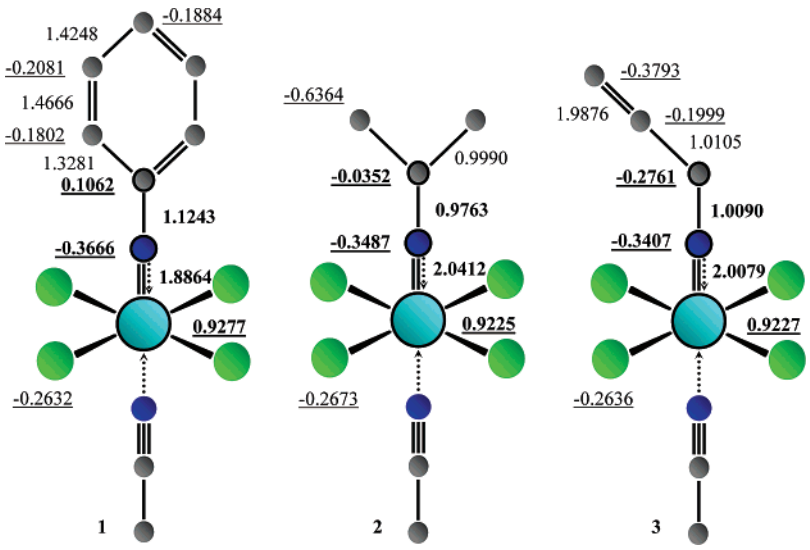

Figure 8. Atomic charges (underlined) from NPA and Wiberg indices for **1**−**3**. Hydrogens are omitted for clarity.

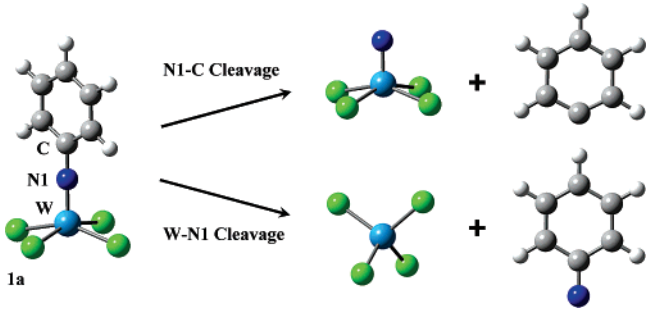

Figure 9. Geometries of the products of W−N1 and N1−C bond dissociation from **2a**.

Table 4. Calculated Bond Dissociation Enthalpy for the N1−C and W−N1 Bonds in **1a**−**3a** and **1a′**−**3a′**

compound	BDE (N1–C) (kcal/mol)	BDE (W–N1) (kcal/mol)
1a	121.3	80.0
2a	98.4	88.2
3a	82.7	86.4
1a′	107.5	85.6
2a′	90.2	94.5
3a′	70.4	93.1

Although the calculated N1−C bond lengths were not significantly different for isopropylimido complex **2a** and allylimido complex **3a** (Table 2), the trends in calculated N1−C bond dissociation enthalpies (BDE) for **1a**−**3a** do differ as a result of the relative stabilities of the organic radicals formed upon homolysis. Note that the metal-containing fragment (Cl_4WN) is the same for all three N1−C cleavages. These differences in BDE for **1a**−**3a** parallel the trend in the reported N−C bond dissociation energies for the corresponding amines R−NH_2 (R = Ph, ^{i}Pr, allyl).[36,37] For both the amines and **1a**−**3a**, the N−Ph BDE is ca. 20 kcal/mol higher than that of N-^{i}Pr. The *N*-allyl bond is weaker than the isopropyl, although the calculated **2a**−**3a** comparison affords a larger difference than found in the amines (15.7 vs 10.7 kcal/mol). The relationship between the estimated N−C BDE for **1a**−**3a** and apparent activation energies for deposition of WN_x films deposited from these precursors[17] suggests that computational estimation of bond dissociation energies could be of value in screening CVD precursors.

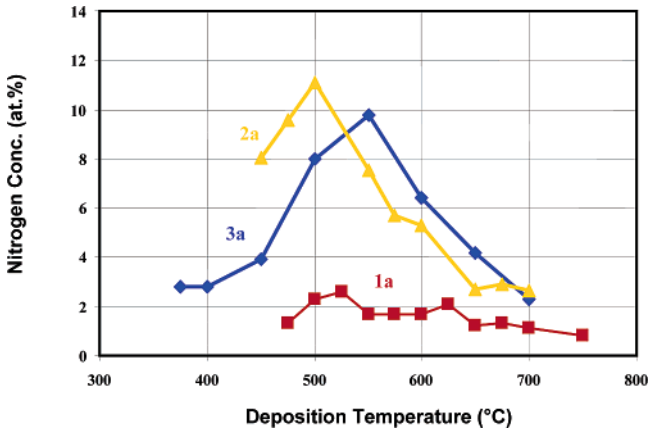

Figure 10. Comparison of nitrogen content in the films grown from **1a**−**3a** (AES). Data are taken from ref 17.

Note that the preceding discussion implicitly assumes that C−N bond cleavage occurs from the tetrachloride complexes $Cl_4W(NR)$ (**1a**−**3a**). Also in Table 4 are the corresponding calculated bond dissociation energies for the hydride complexes $Cl_3HW(NR)$ (**1a′**−**3a′**), the products of the first σ-bond metathesis reactions of **1a**−**3a** with H_2. Conversion to the hydride complex strengthens the W−N bond while weakening the N−C bond in each complex. Since these changes would facilitate C−N cleavage, it is certainly possible that dissociation of the imido substituent occurs after some or all of the chlorides are exchanged for hydride.

The computational results can be qualitatively correlated to the nitrogen content of films grown from **1a**−**3a** (Figure 10). Note that that the concentration values shown in this figure are derived from AES measurements using elemental standards, and thus only the relative trends are meaningful. The relatively low W−N bond strength of phenylimido complex **1a** with respect to alkylimido complexes **2a** and **3a** suggests that the phenylimido ligand is more likely to dissociate from the metal intact. This loss of the PhN moiety would result in lower nitrogen content in films from **1a** as seen in Figure 10.

(36) Benson, S. W. *Thermochemical Kinetics*, 2nd ed.; Wiley-Interscience: New York, 1976.
(37) Luo, Y.-R.; Holmes, J. L. *J. Phys. Chem.* **1994**, *98*, 303−312.

Conclusions

In this study, we used experimental kinetics, DFT calculations and statistical thermodynamics to evaluate reaction pathways for growth of WN_x films from the phenylimido complex $Cl_4(CH_3CN)W(NPh)$ (**1**), the isopropylimido complex $Cl_4(CH_3CN)W(N^iPr)$ (**2**), and the allylimido complex $Cl_4(CH_3CN)W(NC_3H_5)$ (**3**). The computational results and experimentally determined activation parameters are consistent with facile dissociation of the acetonitrile ligand (CH_3CN) from **1**−**3** in the temperature range used for CVD. Computational study of reaction of the coordinatively unsaturated complexes **1a**−**3a** with H_2 located possible transition states for chloride loss via σ-bond metathesis with hydrogen to yield HCl, the experimentally observed chlorine-containing product in the reactor effluent. Finally, through qualitative and quantitative theoretical analyses for N(imido)−C and W−N(imido) bonds, nitrogen content in the films grown from **1**−**3** is linked to calculated bond dissociation energies. Further computational and experimental studies are underway.

Acknowledgment. We thank the National Science Foundation for support under NSF-CRC grant CHE-0304810. We also thank Prof. Adrian E. Roitberg for valuable discussion concerning calculations.

Supporting Information Available: Complete citation for ref 18, table of rates for the acetonitrile exchange in complex **2** and plot of ln(k/T) vs 1/T. This material is available free of charge via the Internet at http://pubs.acs.org.

JA0621804